Hindawi
Advances in Civil Engineering
Volume 2022, Article ID 5888020, 20 pages
https://doi.org/10.1155/2022/5888020

Research Article

Integrating Intrinsic and Eccentric Seismic Vulnerability Indices to Prioritize Road Network Accessibility

Ahmad Mohamad El Maissi,[1] Sotirios A. Argyroudis,[2] Moustafa Moufid Kassem,[1] Lee Vien Leong,[1] and Fadzli Mohamed Nazri[1]

[1]*School of Civil Engineering, Engineering Campus, Universiti Sains Malaysia, 14300 Nibong Tebal, Penang, Malaysia*
[2]*Department of Civil and Environmental Engineering, College of Engineering, Design and Physical Sciences, Brunel University, London UB8 3PH, UK*

Correspondence should be addressed to Fadzli Mohamed Nazri; cefmn@usm.my

Received 4 June 2022; Accepted 5 July 2022; Published 10 August 2022

Academic Editor: Qian Chen

The main aim of this article is to shed light on the establishment of more resilient road networks, which can operate and interact regularly with the surrounding complex-built environment systems during various natural hazards such as earthquakes. This study is integrating engineering judgment and numerical methods to create a comprehensive evaluation for assessing the accessibility rates for road networks. Moreover, it is validating the significance of integrated seismic assessment on various critical sectors in society, such as improving emergency accessibility and adapting improved mitigation strategies for communities that live in disaster-prone districts. In this respect, this article investigates the seismic vulnerability assessment results, aiming at underpinning the understanding of road network risks by discussing the main results of the calculated probability of damage for various parameters of the roadway and its assets. A comparative study is performed to study the effect of spatially variable ground motions at different damage states for the main investigated four parameters. These extracted comparative results are used for weighting the main parameters to calculate the intrinsic seismic vulnerability index scores. Furthermore, the eccentric seismic vulnerability index is calculated, by following different steps such as assessing the calculated debris width resulting from the collapsed buildings and extracting the accessibility rates through concluding the effective width values. Subsequently, the variation between the accessibility rates is investigated and the integrated seismic risk assessment for a road system is developed with a focus on the integration between asset damage and functionality by generating integrated heat maps that take into consideration the correlation between all the developed vulnerability indices.

1. Introduction

The term "built environment" refers to a human-made ecosystem that gives the community identity and meaning in relation to its surroundings [1]. The built environment represents how a community interacts with the natural environment; for example, during earthquakes, it affects the number of deaths, injuries, and property damage. Consequently, it is necessary to analyze the built environments and reduce the amount of seismic damage [2, 3]. The concept of the "built environment" has more recently come to the attention of those conducting research on vulnerability; nevertheless, it has been considered within the more generic domain of "physical vulnerability" [4, 5]. The vulnerability of a wide variety of urban structures with physical aspects, including buildings, municipal infrastructure, networks, and safety infrastructures, has been investigated on an individual basis. Indeed, it is essential to acknowledge that these elements do not exist in isolation from each other, and they interact systemically to produce the disaster effect in the face of a seismic event [6, 7].

Yet, in terms of disaster risk reduction, urban planning needs to be integrated into risk analysis tools [8]. Examining seismic response for complex-built environment systems is a

new study subject. Most of the previous studies concentrated on assessing the physical vulnerability of one parameter, such as the surrounding environment, road networks, transportation systems, or urban and emergency infrastructure services. However, it is crucial to integrate various parameters of the complex-built environment into the assessments. In addition, studies that consider more than one parameter are minimal and limited, compared to studies that analyze the seismic physical vulnerability of a specific or individual attribute in complex-built environment systems.

In previous studies, several frameworks used to evaluate the physical seismic vulnerability and resilience of critical infrastructures (CIs), and other subsystem of a community has been the subject of numerous studies. For example, Andrić and Lu [9] analyzed the seismic vulnerability and resiliency of a critical bridge that is situated in the state of California in the United States. The seismic hazard analysis, the bridge fragility analysis, and the seismic resilience evaluation are all components of the fuzzy framework that was utilized for this study. Another seismic vulnerability framework had been presented by C. Huang and S. Huang [10] for the reinforced concrete bridges that were at risk of being damaged by earthquakes. The physical vulnerability model, the restoration model, and the resilience analysis are the three components that are included in the framework. The physical vulnerability model was used to get the probability of damage to the bridge piers for given seismic intensities, while the restoration model was utilized to evaluate the functioning of the aging bridges. Sun et al. [11] used agent-based modelling to assess the seismic susceptibility of France's Luchon Valley road network. In the study, critical road network bridges were chosen to classify the earthquake resistance design for the investigated transportation systems. Shang et al. [12] have presented a quantitative framework that was created based on the Chinese seismic design code in order to evaluate the seismic resilience of the hospital systems in China (GB 20011–2010). The framework took into account the hospital's seven most important subsystems, which are the structural system, the electrical components, the mechanical structure, the water supply and sewage system, the healthcare system, and the evacuation system. The evacuation system of a road network is based on the emergency cars and how much they can be appropriate to be used in the emergency evacuation process during earthquakes. Moreover, Kassem [13] established a uniform seismic vulnerability index (SVI) framework for reinforced concrete building typology. This framework has been validated and investigated through the process of evaluating the seismic behaviour of hospital and school reinforced concrete buildings in Malaysia. During this process, the authors proposed a seismic vulnerability index by using nonlinear parametric analysis (NL-PA) in order to prioritize the damage to the buildings, in which this index was used to classify the severity of the damage to the buildings. These studies are used to determine the main typologies and the expected collapse ratios for the investigated buildings in this research [14, 15].

The approaches that investigate the physical vulnerability of road networks can be divided into two primary classifications. The first one is based on the Intrinsic Seismic Vulnerability Index (ISVI), which effectively addresses the evaluations of the components that are formulating the system itself such as pavement, embankments, and soil beneath roadway. The second one provides an evaluation of external influences that could disrupt the road system network through the Eccentric Seismic Vulnerability Index (ESVI). These factors or influences include the space that surrounds buildings, pylons, telecommunication towers, and others. The majority of the existing research on road networks focuses entirely on either the ISVI or the ESVI as their primary variable of interest.

As an example, Adafer and Bensaibi [16] studied the vulnerability of Algeria's road networks to seismic events using an ISVI model based on empirical data derived from seismic experts around the world and data extracted from previous earthquakes in Algeria, in order to use this method in weighting the road network's assets. The research team concentrated their attention in this study on the evaluation of the potential material damage that earthquakes could inflict upon roadways. On the other hand, several studies focused on the ESVI in order to investigate the influence of the natural setting of the surrounding environment on the susceptibility of roadways. Costa et al. [17] developed a probabilistic approach to evaluate the consequences of earthquakes on road traffic by analyzing the correlation between the physical damage to roadway systems and traffic flow of the urban road network of Messina, Italy. The spatial variance of seismically induced damage to buildings that can cause closure to roads was taken into consideration using a probabilistic approach. By comparing traffic behaviour on the road network in normal conditions and in the event of building debris, this study was able to determine the road network's functionality. Furthermore, Ertugay et al. [18] produced an accessibility model based on the probability of road closures in Thessaloniki, Greece, with maps depicting the impact of earthquake scenarios on the accessibility of specified shelter spots. Moreover, Argyroudis et al. [19] performed a risk assessment for road networks considering the interaction with the built environment in the surrounding area. This study's primary objective was to generate a probabilistic systemic risk analysis to evaluate the connectivity of the road network affected by debris caused by collapsed buildings along the roads.

Numerous studies have utilized the ESVI of road networks in order to evaluate the physical damage, accessibility to vital service centres, or interconnection of road networks (i.e., trip time and distance). These evaluations have been carried out for the purpose of determining whether or not the road networks are linked [20–26]. Nevertheless, several studies have also examined how buildings and roadways interact, with particular attention paid to traffic flow and reliability in an emergency [20, 27, 28]. In contrast, there are a few works that focus on street network punctual conditions and debris interactions, and only a few of them feature historical earthquake scenarios [29, 30].

Indeed, the research is still deemed to be quite restricted when it comes to the concept of an integrated seismic risk assessment approach that correlates the ISVI and ESVI to analyze the road network in a complex-built environment. Yet, the United Nations sustainable development goals (SDGs) such as SDG9 and SDG11 call for resilient, secure, and sustainable communities, and this will be achieved by reducing the risk of critical infrastructure to natural disasters such as earthquakes, and minimizing their consequences for the society and economy reducing deaths and injuries [13, 31, 32].

These studies highlight the need for an integrated seismic vulnerability assessment strategy for complex-built environments that considers the link between internal and extrinsic system properties. Regarding improving resilience and enhancing emergency access for certain urban built environment systems, this integrated approach is regarded as a critical first step. In this article, a comparative study is carried out to study the effect of different hazard scenarios that are considered with the spatial distribution of seismic intensities (VIII and IX) on each of the four main investigated parameters (P1: Embankment Height; P2: pavement strength; P3: soil type; and P4: number of lanes), which aims at improving the understanding of road network risks by addressing the determined probability of damage for the investigated parameters. These comparative results are utilized to weight the main parameters for the ISVI scores. In addition, the Eccentric Seismic Vulnerability Index (ESVI) is computed by first determining the calculated debris width (W_d) as a consequence of the collapsed buildings and then determining the accessibility rates by drawing conclusions about the effective width values (W_{eff}). Eventually, this aforementioned information is then used to develop an integrated seismic risk assessment for a road system, which considers the correlation between the various developed vulnerability indices and generates integrated heat maps that take into account the correlation between the various vulnerability indices.

This research is considered an original framework for building an analytical investigation approach and combining both Intrinsic and Eccentric Seismic Vulnerability Indices (ISVI and ESVI), in terms of internal and external factors of the roadway system to improve the established methods that have been done in past studies. The proposed approach for the ISVI is based on an analytical investigation that quantifies, for the first time in the literature, the impact caused by a parameter's physical performance on the road behaviour based on different earthquake scenarios and the probability of damage for each parameter of the roadway system that can be integrated uniformly into risk-based strategies. This step helps in prioritizing the parameters from the most to the least essential one, based on the results of the probability of damage for the roads. Moreover, the developed framework is considered significant due to the fact that it is building heat maps to find the correlations between the ISVI and the ESVI, where the past research focuses on assessing solely the internal or external factors, without investigating the effect of the integrated index on the accessibility rates.

2. Investigated Roads and the Main Surrounding Buildings

A small area is chosen in the southern-west part of Penang, Malaysia, as a case study. The road network under investigation contains 16 different roads and 29 intersecting nodes as shown in Figure 1. The investigated roads are classified as secondary and urban collector roads. Additionally, all roads are considered one-way roads because in case of earthquakes, the emergency vehicles may not follow the normal traffic regulations. The main parameters used in this study for each street include the width of road that is ranging between 3.8 m and 11 m with two main conditions building facing street from one side or from both sides of the road as shown in Table 1. The zoning of a sample street is shown also in Figure 1, where the street is divided into three main zones based on the buildings facing the road from two sides.

Figure 1 shows the roads surrounded by the classified buildings, where they are classified on the basis of buildings height that is ranging between 6.5 and 34 meters. Moreover, the building depth and volume values are specified for the calculation of the width of debris resulting from the collapsed buildings. The building depth range between 10.13 and 26.91 meters. The height and depth of the buildings are determined based on field investigation, while the ranges of building volume values are calculated based on the determined height, width, and depth of the building by taking into consideration the void volume inside the building. The volume of buildings ranges between 1025.78 m^3 and 5315.56 m^3. The 37 buildings that are under investigation in this application are categorized into low-rise building (LRB), mid-rise building (MRB), and high-rise building (HRB) based on the determined heights as shown in Figure 1 and Table 2.

3. Assessment of Roadway System Resistance Based on the Intrinsic Seismic Vulnerability Index (ISVI) and Eccentric Seismic Vulnerability Index (ESVI) Approaches

To assess the resistance of roadway systems, two different approaches are developed. The first approach is developed based on the Intrinsic Seismic Vulnerability Index (ISVI) that takes into consideration four intrinsic main parameters (P1: embankment height, P2: pavement strength, P3: soil type, and P4: number of lanes) of the roadway system. These parameters are investigated with respect to the calculated probability of damage (POD) for varying ground motions at different damage states. The cumulative distribution function (CDF) assessment approach is used to calculate the POD values for different ground motions that are shown in Table 3 by using Equation (1), which was downloaded from the Consortium of Organizations for Strong-Motion Observation Systems (COSMOS) database and Pacific Earthquake Engineering Research (PEER) database. The POD values are extracted at two different fixed intensities for different Sa values VIII (0.5 g and 0.8 g) and IX (1.0 g and 1.3 g). After that, a comparative study is performed to compare the main values of POD for different parameters at different damage states (DSs) as shown in Table 4:

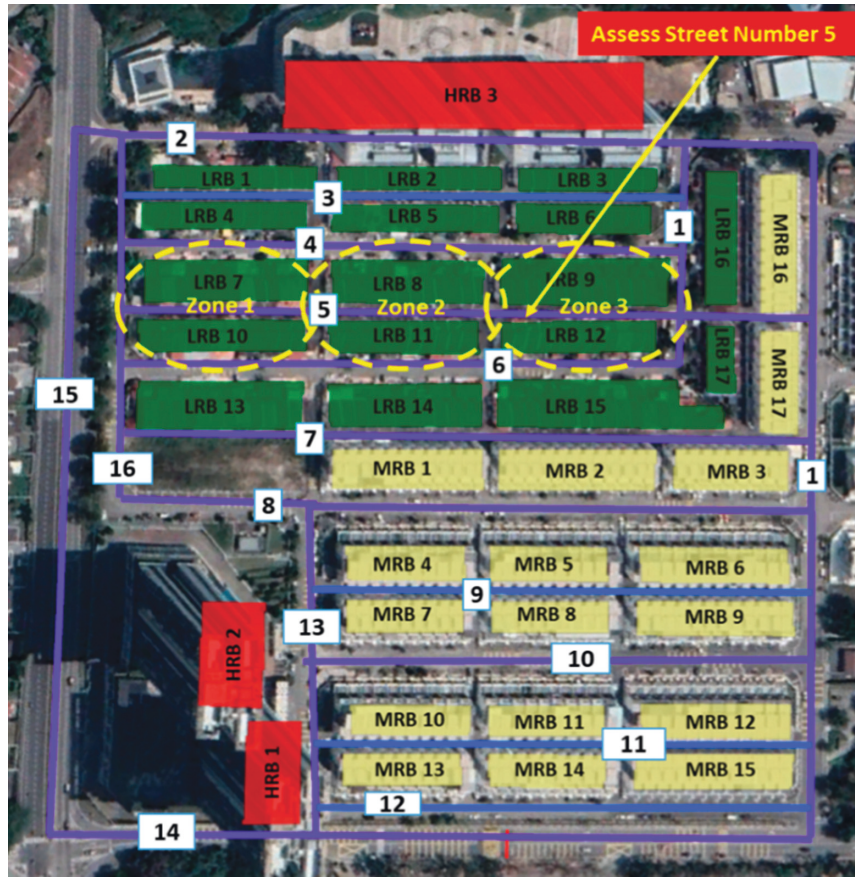

Figure 1: Map for categorized buildings and streets under investigation.

Table 1: Description of road network main parameters.

Street number	Street width (m)	Number of lanes	Buildings facing one side of road	Buildings facing two sides of road
1	8.80	2	x	—
2	12.31	4	—	x
3	3.28	1	—	x
4	7.00	2	—	x
5	5.00	1	—	x
6	7.81	2	—	x
7	3.15	1	—	x
8	6.30	2	—	x
9	7.64	2	—	x
10	3.76	1	—	x
11	4.38	1	—	x
12	7.5	2	x	—
13	9.04	2	—	x
14	13.00	4	—	—
15	11.79	4	—	—
16	7.50	2	x	—

$$P\left[\frac{\text{Damage} \geq \text{DS}}{\text{Sa}(T1)}\right] = \Phi\left(\frac{\ln\left[\text{Sa}(T1)\right] - \mu}{\sigma}\right), \quad (1)$$

where $\text{Sa}(T1)$is the spectral acceleration for a specific vibration period, Φ is the standard normal distribution, μ is the mean value for damage states, and σ is the standard deviation for each damage state [13].

The extracted result from the comparative analysis is used to determine the effectiveness of the investigated parameters where the results will show the prioritized parameters on the basis of their effectiveness on the roadway system during earthquakes. This is followed by weighting the parameters by using the analytical hierarchy process (AHP) method that is developed by Saaty [34] with respect to their

Table 2: Parameter values of main buildings.

Building ID	Building height, H (m)	Building depth, W (m)	Building volume, $V(m^3)$
LRB 1	7.00	11.13	1232.84
LRB 2	6.50	11.21	1143.35
LRB 3	7.00	10.13	1025.78
LRB 4	7.40	12.05	1403.19
LRB 5	6.50	12.00	1187.68
LRB 6	7.40	12.62	1124.65
LRB 7	8.60	20.38	1572.60
LRB 8	8.60	20.69	1528.57
LRB 9	8.60	21.55	1677.00
LRB 10	7.40	14.38	1338.51
LRB 11	7.40	15.06	1218.04
LRB 12	8.60	15.46	1445.83
LRB 13	10.00	20.79	1873.00
LRB 14	10.00	20.87	1775.40
LRB 15	8.60	21.12	1764.90
LRB 16	10.00	12.76	1564.80
LRB 17	10.00	12.22	845.20
MRB 1	12.90	18.85	2227.83
MRB 2	12.90	18.66	2339.28
MRB 3	12.90	18.58	1813.99
MRB 4	17.20	22.48	2621.97
MRB 5	17.20	22.40	2594.10
MRB 6	12.90	22.44	2303.94
MRB 7	15.00	15.86	2055.31
MRB 8	12.00	14.68	1636.80
MRB 9	12.00	15.68	2000.64
MRB 10	15.00	14.00	2007.00
MRB 11	14.40	13.88	1892.16
MRB 12	14.40	18.47	2552.25
MRB 13	17.20	16.48	2400.09
MRB 14	15.00	15.92	2039.40
MRB 15	17.20	16.19	3026.17
MRB 16	17.20	18.35	2772.65
MRB 17	17.20	18.88	2210.54
HRB 1	34.00	25.38	4806.92
HRB 2	34.00	26.91	5315.56
HRB 3	34.00	18.64	50254.72

Table 3: Selected sets of ground motion records.

No.	Earthquake	Year	Station	PGA (g)	Epicentral distance (km)	Magnitude (Mw)
1	Izmit-Kocaeli, Turkey	1999	Nuclear Research Center	0.181	101	7.4
2	Landers USA	1992	San Bernardino, CA	0.332	80	7.3
3	Superstition Hills, USA	1987	Calipatria, CA	0.252	27	6.5
4	Chi-Chi, Taiwan	1999	Taichung	0.527	39	7.6
5	Loma-Prieta, USA	1989	Emeryville, CA	0.490	68	7.0
6	Northridge, USA	1994	Santa Monica, CA	0.684	28	6.7
7	Ranau, Sabah, Malaysia	2015	KKM_HNE	0.125	65	6.1

Table 4: Damage States of Roadway and its Assets (Argyroudis and Kaynia [33]).

Serviceability	Damage states (DS)	Direct damages	Indirect damages
Fully or partially closed due to temporary maintenance and traffic for few weeks or few months.	Extensive	Major settlement or offset of the ground (>60 cm)	Considerable debris of collapsed structures
Fully closed due to temporary maintenance for few days. Partially closed to traffic due to permanent maintenance for few weeks.	Moderate	Moderate settlement or offset of the ground (30 to 60 cm)	Moderate amount of debris of collapsed structures
Open to traffic. Reduced speed during maintenance.	Minor	Slight settlement (<30 cm) or offset of the ground	Minor amount of debris of collapsed structures
Fully open.	None	—	No damage/Clean road

effectiveness rates as described in detail in Section 3.2. Subsequently, the ISVI scores are calculated from the extracted weights and the presented parameters for each road.

The ESVI is the second approach considered in this research to study the effect of extended debris from the collapsed surrounding buildings on the disruption of accessibility rates for the road network. The debris width W_d values are calculated using (2) and (3) based on two types of collapses that are represented in Figures 2(a) and 2(b) that is adopted from Argyroudis et al. [19]. The developed methods based on the integration between the ISVI and ESVI scores are considered more reliable when compared to previous studies that tackled the vulnerability assessment of road networks. This is due to the fact that the developed methods in this research are built on the basis of analytical investigations. On the other hand, empirical approaches have the limitation of information availability, while an empirical study requires large input data that might be impossible to collect in many developing countries [16]. Nevertheless, the main disadvantage that is related to the analytical approach is the high computational effort that is needed compared to empirical methods. Subsequently, due to the numerous variables, establishing an accurate integrated seismic risk assessment is a challenging approach. However, a model that incorporates intrinsic and eccentric parameters is necessary for a more accurate risk assessment of road networks:

$$W_d = \sqrt{\frac{2K_v \times W \times L}{\tan c}} - L, \tag{2}$$

$$W_d = \sqrt{W^2 + \frac{2K_v \times W \times H}{\tan c}} - W, \tag{3}$$

where W is the building width, K_v is the collapse ratio of the building, L is the building length, Y is the building height, and c is the collapse angle based on Argyroudis et al. [19].

Effective width W_{eff} that represents the accessible areas that are not obstructed by the debris of the collapsed buildings is calculated based on the resultant W_d values for the two types of collapses. The following equation is used to calculate the values of W_{eff}:

$$W_{\text{eff}} = W_r - W_d, \tag{4}$$

where W_{eff} represents the effective width of the road that vehicles can pass through, W_r is the width of road, and W_d is the width of debris resulting from building destruction.

Subsequently, the ESVI scores are calculated for two types of emergency vehicles: normal emergency vehicles (NEVs) and emergency service vehicles (ESVs) at a different intensity of (VIII) and for the intensity of (IX) with respect to the W_{eff}values as shown in using Equation (5). The NEV and ESV have a different manoeuvring limit, where the NEV is considered wider (3.5 m) when compared to the ESV (2.5 m):

$$\text{ESVI} = 100 - \frac{W_r - \left(W_{\text{eff}(L)} + W_{\text{eff}(R)}\right)}{W_r}, \tag{5}$$

where W_r represents the road width, $W_{\text{eff}(L)}$ effective width for the left side, and $W_{\text{eff}(R)}$ effective width for the right side.

3.1. Analysis of the Effect for Spatially Variable Ground Motions at Different Damage States. For conducting the analysis of the effect of the spatially variable ground motions on the damage of road networks and their assets, different earthquake intensities and different average spectral acceleration (Sa) are considered. For the intensity of VIII, the Sa is fixed at 0.5 g and 0.8 g. Meanwhile, for the intensity of IX, the Sa values are fixed at 1.0 g, and 1.3 g, respectively. The main specified intensities are selected based on their criticality and due to the fact that the values of these intensities are showing the variation gaps when compared to smaller intensity ranges and are reflecting the main aim of the seismic vulnerability analysis. After assessing the main investigated parameters for roadway and their assets at each specified earthquake intensity, the results of the probability of damage are extracted and distributed at each damage state. The variation in the probability of damage at each damage state for the assessed performance of each parameter at different seismic intensities is shown in Figures 2–5.

3.1.1. (P1): Embankment Height. The extracted results from the vulnerability assessment of embankment on the basis of the height difference show a high variation in the probability of damage at different damage states. It could be found that as the seismic intensity is increasing from 0.5 g to 1.3 g, the probability of damage is increasing gradually at all damage states as shown in Figure 3. For instance, the probability of damage values of embankments for all various heights at 0.5 g (VIII) and 0.8 g (VIII) that are demonstrated in Figures 3(a) and 3(b), the procedure of using an identical ground motion at the same earthquake intensities is overrating the occurrence of the probability of damage at minor state, and this is resulting in underestimating the occurrence of damage at moderate and extensive states. On the other hand, the probability of damage for the various embankment heights at 1.0 g (IX) and 1.3 g (IX) is given in Figures 3(c) and 3(d). The results are showing the same trend but for different damage states, where it is overrating the occurrence of the probability of damage at minor and moderate states, and this is resulting in underestimating the occurrence of damage at the extensive state. All that reveals that lower intensities give high ratings to the minor states compared with the moderate state, while higher intensities provide more ratings for minor and moderate states with less consideration for extensive damage. Mainly, Figures 3(a)–3(d) are reflecting the main results of the probability of damages through using cumulative distribution function (CDF) by showing that embankments with greater heights tend to have a high probability of damage in comparison with embankments with lower heights. Moreover, the results are showing high fluctuation rates between different classes that indicates the high effectiveness of this parameter on the roadway system.

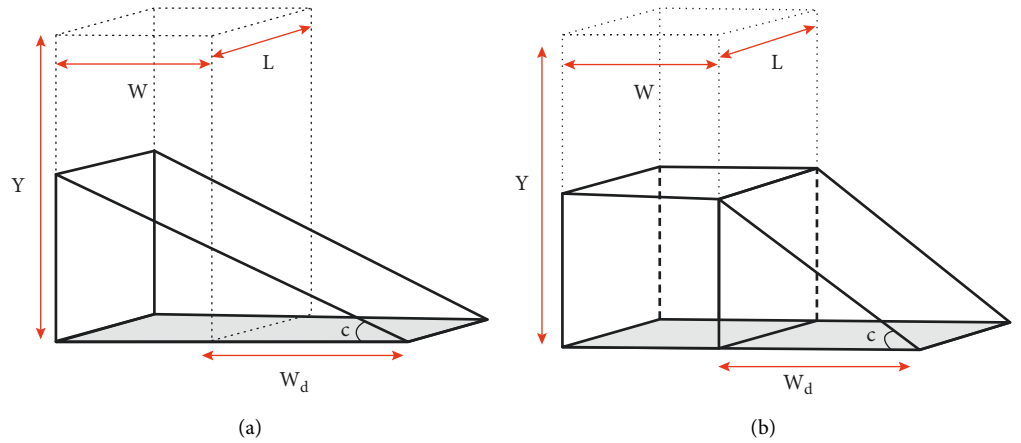

Figure 2: (a) Building collapse type 1. (b) Building collapse type 2 based on Argyroudis et al. [19].

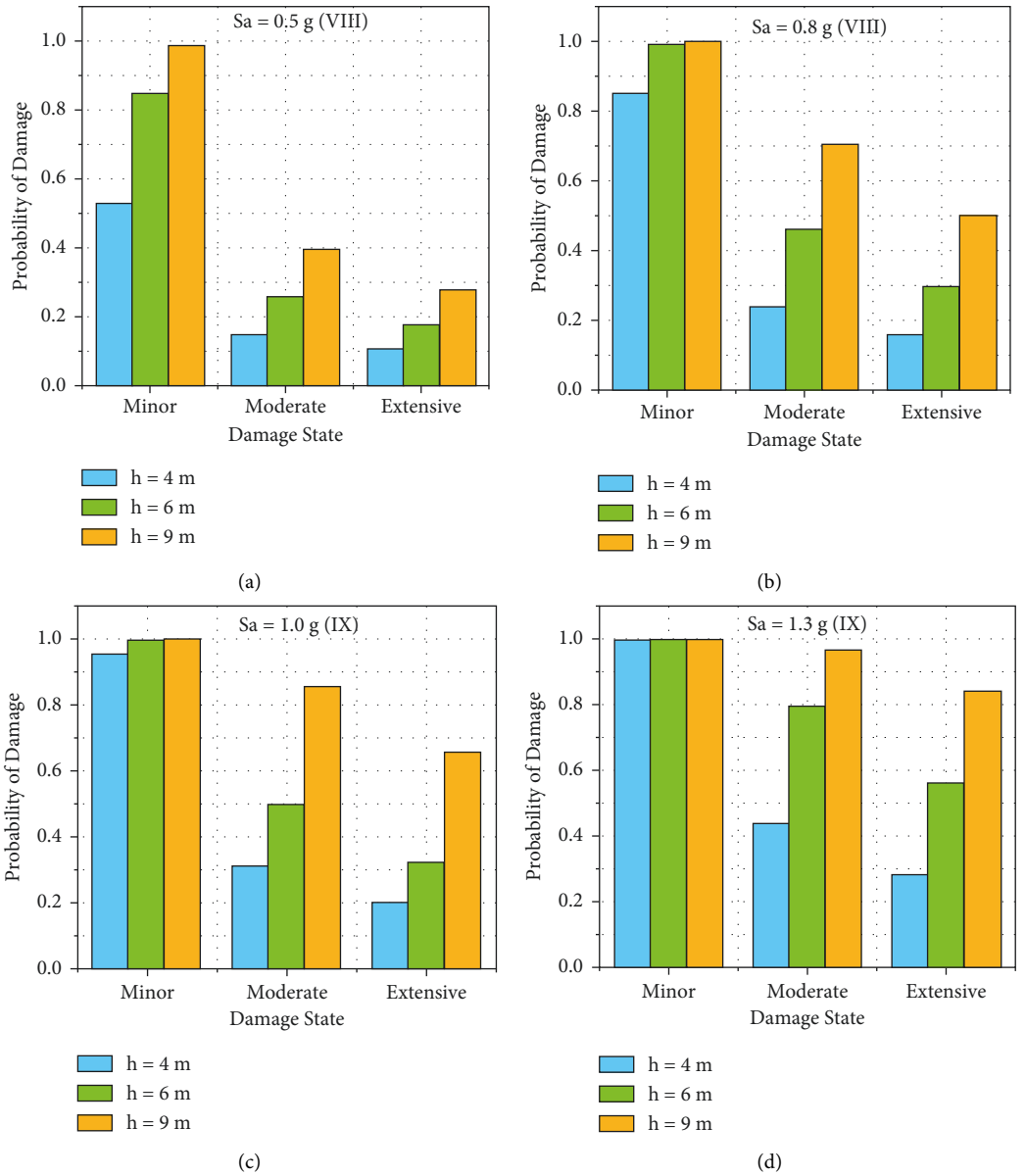

Figure 3: Damage probability for embankment with different heights (P1) for various damage states and seismic intensities.

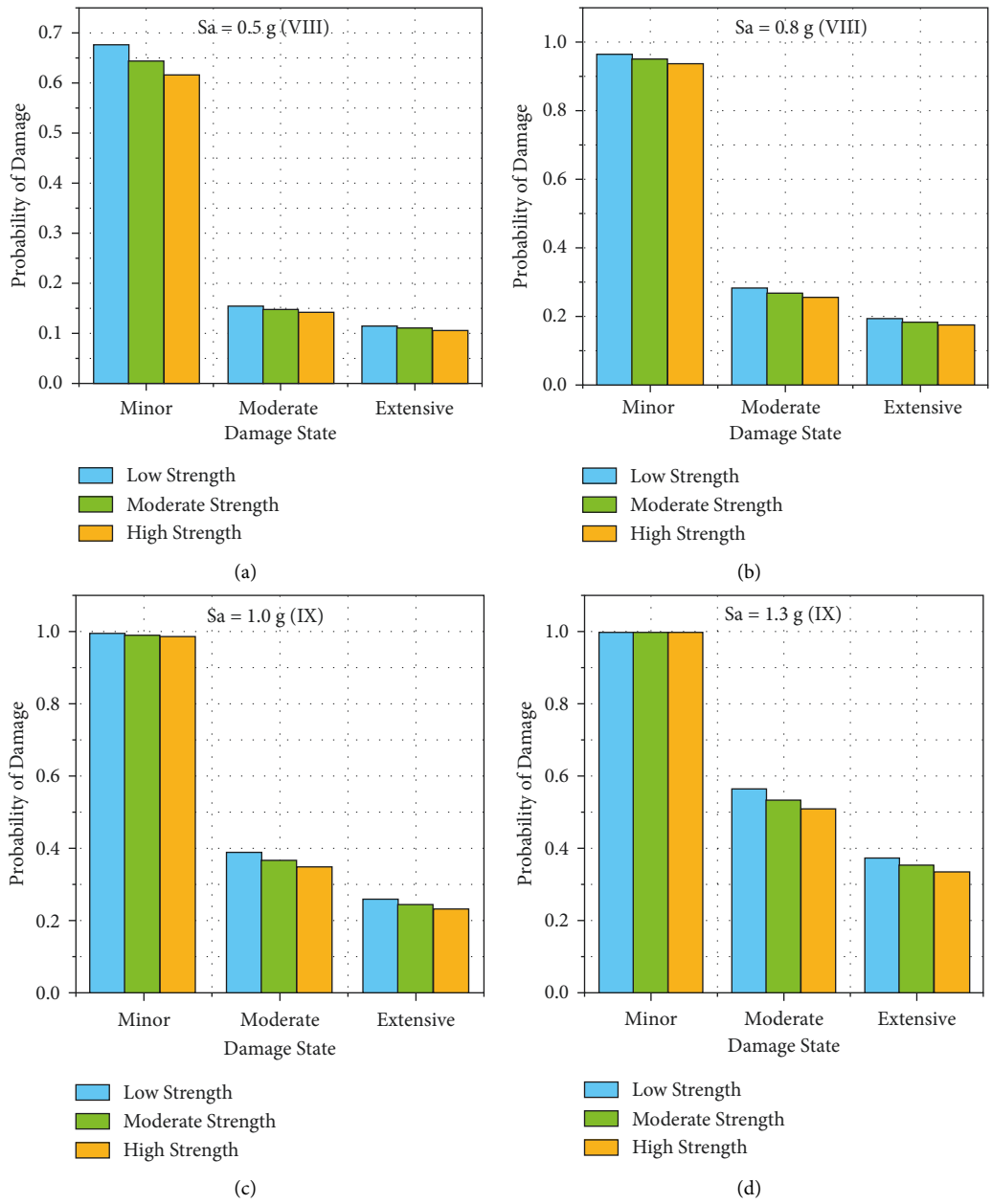

Figure 4: Damage probability for roads with different pavement strength (P2) for various damage states and seismic intensities.

3.1.2. (P2): Pavement Strength. The vulnerability assessment results for the roadway assets based on the pavement strength shows a high difference of the probability of damage values at different damage states, especially when considering the minor state compared with the other two damage states. Although a similar case is shown between the minor and moderate states as demonstrated in the vulnerability assessment for the height of embankments, it is clear that the results vary slightly between moderate and extensive damage states at all seismic intensities, as shown in Figures 4(a) and 4(b). A high variation in the probability of damage is clearly represented with a difference higher than 0.6 (60%) when comparing the results between minor and moderate states at all intensities, where it can be seen slightly higher at 1.0 g (IX) and 1.3 g (IX) as shown in Figures 4(c) and 4(d). On the contrary, the variation in the probability of damage between the moderate and extensive states is considered low with a difference less than 0.2.

This is due to the fact that the pavement strength is influencing the roadway vulnerability slightly, since this comparison is clearly indicating that the pavement strength effect is considered critical at minor damage state. However, this effect is considered low for moderate and extensive damage states, where, only at high seismic intensities, the probability of damage can be considered more effective for moderate and extensive states as shown in Figure 4(d). Hence, roadways with lower pavement strength are showing higher vulnerability rates in comparison with roadways with higher pavement strength.

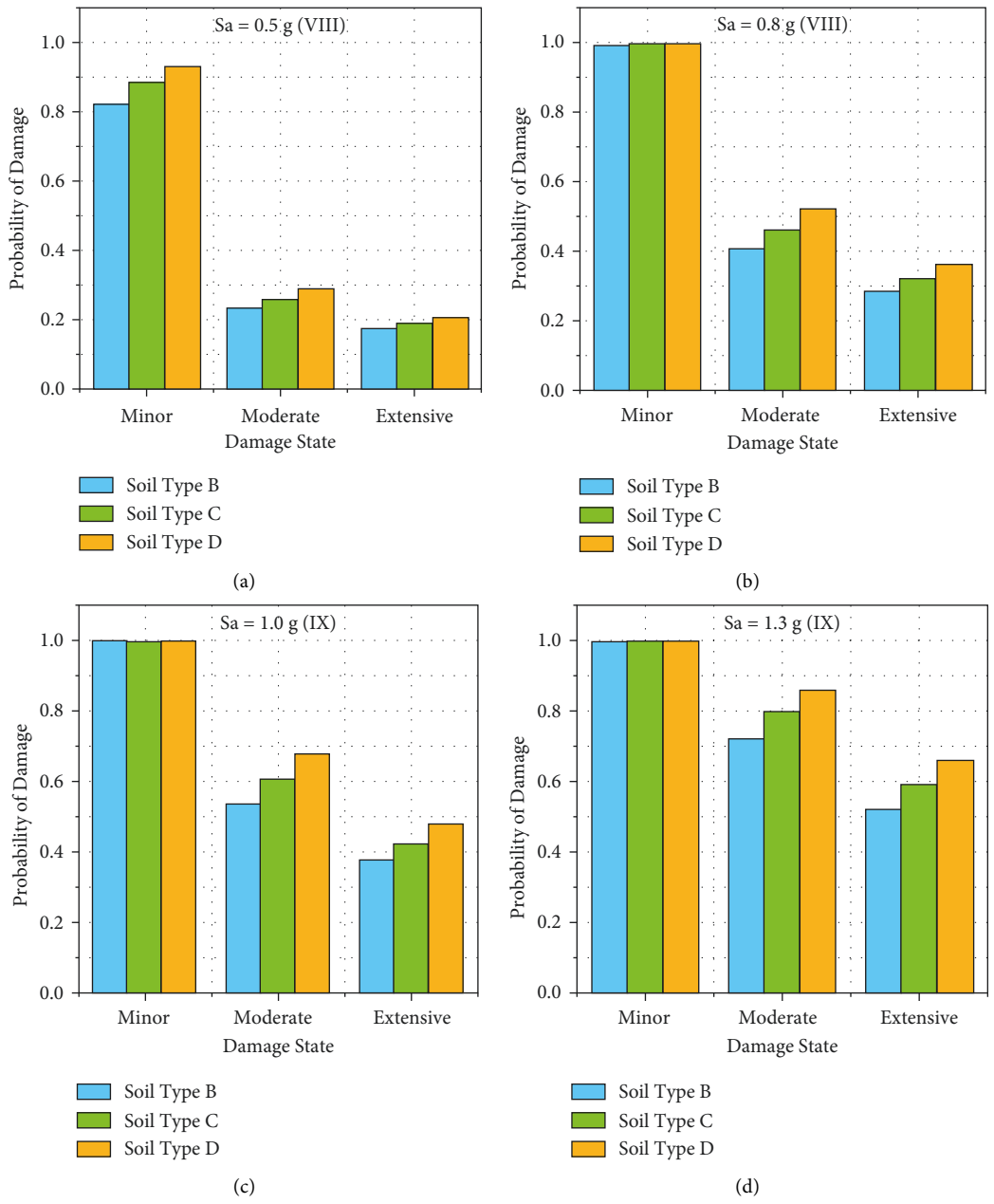

Figure 5: Damage probability for roads with different soil type (P3) for various damage states and seismic intensities.

3.1.3. (P3): Soil Type. The results of the vulnerability assessment of roadway and its assets based on the soil type beneath the roadway system for different seismic intensities at different damage states are showing a high variation with a difference value ranging between 0.5(50%) and 0.7(70%), when comparing the probability of damage at the minor state with moderate and extensive states at intensities of 0.5 g (VIII) and 0.8 g (VIII) as shown in Figures 5(a) and 5(b). Nevertheless, the results are also illustrating a small variation between the probabilities of damages, with a difference value ranging between 0.3 (30%) and 0.4 (40%) as shown in Figures 5(c) and 5(d).

These results clearly show that the soil type is more significant at minor damage states, but it can also moderately affect moderate and extensive damage state occurrences. The probability of damage value distribution at different damage states is fluctuating gradually between different classes (soil types B, C, and D). This indicates that the soil type is considered a moderately effective parameter for the vulnerability of roadway systems.

3.1.4. (P4): Number of Lanes. The assessment of roadway and its assets based on the variation in the number of lanes is showing a great difference in the extracted results, where the difference can be seen clearly high with values ranging between 0.5(50%) and 0.7(70%), when comparing the results at the minor state with the moderate and extensive states

especially at 0.5 g (VIII), 0.8 g (VIII), and 1.0 g (IX) intensities as shown in Figures 6(a)–6(c). However, Figure 6(d) at 1.3 g (IX) is illustrating a sharp increase in the probability of damage at moderate and extensive states in comparison with the results of lower intensities that are shown in Figures 6(a)–6(c). This is due to the fact that the number of lanes can have a higher effect on the roadway system at higher seismic intensities when compared to lower intensities. In addition, the results have shown a small variation when assessing different roadway systems with various number of lanes classes (<2 lanes, = 2 lanes, >2 lanes) at different seismic intensities as represented in Figures 6(a)–6(d).

Subsequently, the road width parameter is being more effective when high seismic intensities are considered, while the variation of classes are gradually affecting the probability of damage for roadway system. All these results indicate that the number of lanes is considered with low effectiveness when compared with the soil type and height of embankment parameters, but still considered slightly more effective when compared to the pavement strength parameter.

3.2. Calculation of the Intrinsic Seismic Vulnerability Index (ISVI) Scores. The Intrinsic Seismic Vulnerability Index (ISVI) scores will be calculated based on the weighting of parameters that is concluded from the comparative analysis for the most influential parameters as described in Section 3.1. After the parameters are prioritized from the most influential one to the least, the weight of each parameter is determined based on the analytical hierarchy process (AHP) method [34] and the scoring pattern done in previous studies [16]. The weights are calculated using a specific matrix model by raising this matrix model to large powers and summing each row and dividing each by the total sum of all the rows. The main calculated weights are 0.50, 0.21, 0.18, and 0.11, and 0.65, 0.21, 0.1, and 0.04 for embankment height, number of lanes, soil type, and pavement strength at the intensity of VIII and IX, respectively. On the other hand, the scores for each parameter are categorized based on their importance as described in previous studies and the number of parameters and their categories that are investigated in this research [16].

Subsequently, the ISVI scores are calculated on the basis of the calculated weights WP_{a_i} and scores S_i for two different seismic intensities and classified as minor damage (0.0–0.4), moderate damage (0.4–0.7), and extensive damage (0.7–1.0) by using Equation (6) and are represented in Figures 7(a) and 7(b)

$$\mathrm{ISVI_j} = \sum_{i=1}^{n} S_i \times WP_{a_i}, \tag{6}$$

where $\mathrm{ISVI_j}$ represents the Intrinsic Seismic Vulnerability Index of the j-th alternative for the road; S_i represents the main scores for each parameter; WP_{a_i} is the i-th of the four weighted parameter; and n is the number of parameters.

Figures 7(a) and 7(b) are clearly showing that the ISVI scores are considered higher at seismic intensity IX when compared to seismic intensity VIII as shown in case of most of the investigated streets; however, when looking at street numbers 3, 6, 9, and 15, the results are decreasing at higher seismic intensity, and this is due to the high weighting rate for the embankment height; thus, when the score of this parameter is decreasing sharply, the ISVI score is decreasing at higher seismic intensities. This variation in the weighting factors is giving the height embankment high effectiveness at seismic intensity IX where the other parameters are negligibly changing the ISVI score especially when considering soil type and pavement strength.

4. Calculated Eccentric Seismic Vulnerability Index (ESVI) Scores for Road Networks Based on the Possibility of Blockage

The values of the Eccentric Seismic Vulnerability Index (ESVI) scores are calculated using (5), where the percentage of blockage is determined. Various scores are obtained based on the effect of debris width that resulted from the collapse of surrounding buildings. All the ESVI scores of the 16 investigated roads are calculated for collapse types 1 and 2, where they are introduced in Figures 8(a) and 8(b).

The ESVI values for the main three investigated zones of roads that are presented in Figures 9–11 are reflecting the results concluded based on ESVI scores, where, based on these ESVI scores, the accessibility rates are considered higher when assessing collapse type 1 in comparison with collapse type 2 at both seismic intensities. Nevertheless, when comparing the ESVI values for collapse types 1 and 2, the higher values are presented in the higher seismic intensity scenario (IX) when it is compared with the (VIII) seismic intensity.

4.1. Representative Figures for the Blocked Zones of Investigated Roads. Representative figures are conducted based on the main values of the extended debris that are extracted from the ESVI values for both types of collapses at different seismic intensities (VIII and IX). Figures 9–11 represent the three chosen samples for the investigated roads from all the 16 investigated roads.

The figures are illustrating the main zones that are considered accessible during earthquakes for emergency vehicles. For instance, in Figure 9, it is clear that zones 2 and 3 for street number 1 will be fully accessible for emergency vehicles, since there is no extended debris from surrounding buildings in these zones. However, when studying the impact of surrounding buildings on zone 1, it is showing an extended debris from buildings MRB-16 and MRB-17 from the left side only. Hence, the results are showing accessible areas for normal emergency vehicles (NEVs) and emergency service vehicles (ESVs) with accessibility distance values of 4.93 m and 3.96 m for collapse types 1 and 2 at the seismic intensity of VIII. On the other hand, when investigating the same zone at higher seismic intensity IX for collapse types 1 and 2, the road is not accessible for both types of emergency vehicles with values less than 2.5 m.

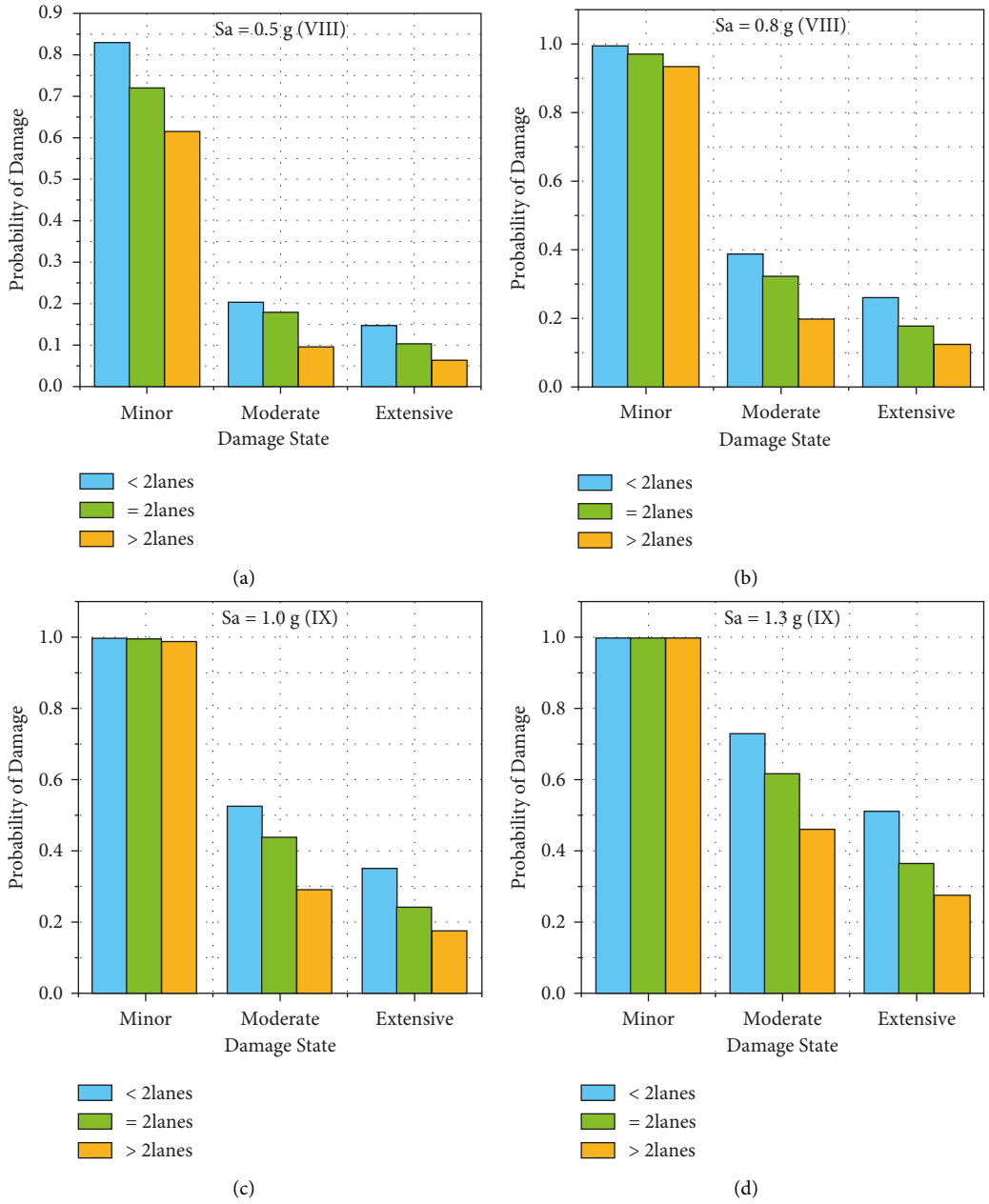

Figure 6: Damage probability for roads with different number of lanes (P4) for various damage states and seismic intensities.

Moreover, in Figure 10, another case for extended debris can be noted, where the debris is represented at both sides of the road for all three zones for street number 4, where in case of collapse type 1 at seismic intensity VIII, the accessible areas are considered efficient for manoeuvring of NEV and ESV at the three zones with accessibility distances ranging between 4.46 m and 4.61 m. On the contrary, collapse type 1 at the seismic intensity of IX and collapse type 2 at the seismic intensity of VIII are showing a smaller accessibility distance at the three investigated zone values ranging between 2.78 m and 3.02 m that considered efficient for manoeuvring of ESV only. Subsequently, for collapse type 2 at the seismic intensity of IX, the accessibility distance becomes very small with entire zones blocked for both types of emergency vehicles. This case is repeated, but with fully collapsed zones as shown in Figure 11.

4.2. Percentage of Variation between Eccentric Seismic Vulnerability Index (ESVI) Values for Collapse Type 1 at Different Seismic Intensities. The percentage of variation is conducted by comparing the Eccentric Seismic Vulnerability Index (ESVI) values for collapse type 1 at two different seismic intensity scenarios (VIII) and (IX), these percentage of variation values are represented in Figure 12 for all the investigated streets. The values are showing a fluctuation between the percentages of variation when comparing the

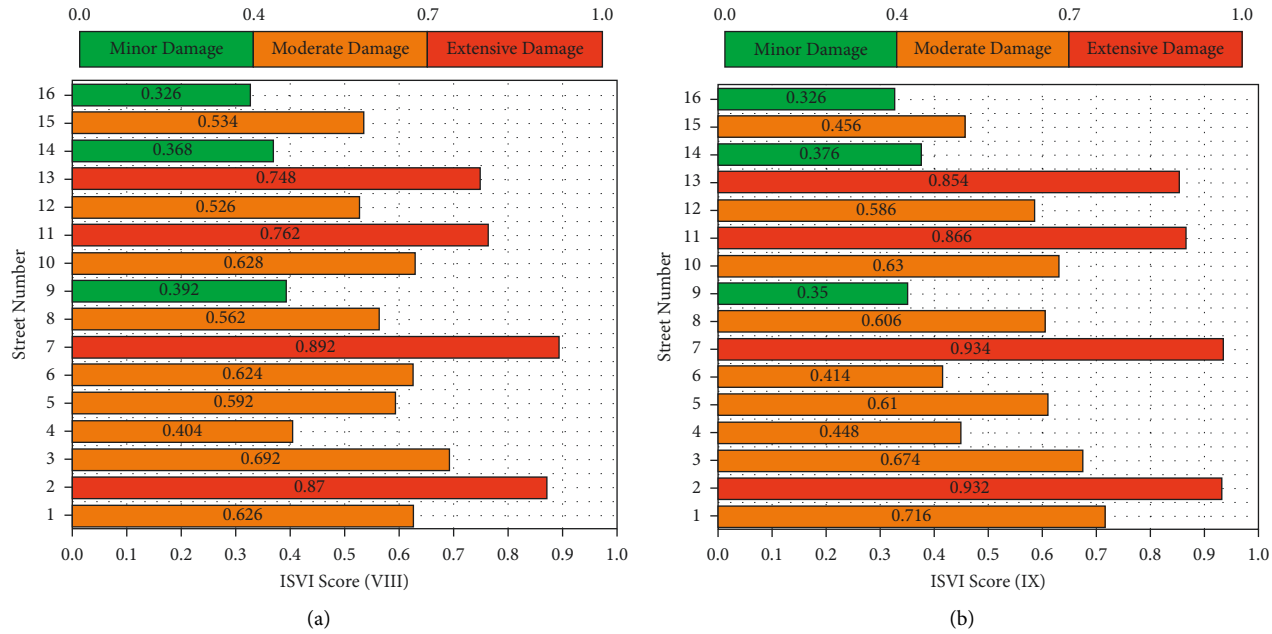

Figure 7: (a) ISVI scores for the investigated streets at seismic intensity (VIII). (b) ISVI scores for the investigated streets at seismic intensity.

investigated roads and their zones, but it is clearly illustrating higher variations for street number 3, 4, and 16 at all three different zones with values ranging between 56% and 73%, this is due to the fact that the buildings surrounding these roads are with high collapse rates, by which they are varying highly between the changing seismic intensity scenarios. On the contrary, some of the values for investigated roads are giving low percentage of variation that in some cases, the values are giving 0%, because the surrounding buildings are not damaged or the ESVI values of these roads are still the same for both seismic intensities.

4.3. Percentage of Variation between Eccentric Seismic Vulnerability Index (ESVI) Values for Collapse Type 2 at Different Seismic Intensities. Figure 13 shows the percentage of variation between the Eccentric Seismic Vulnerability Index (ESVI) values for collapse type 2 based on two seismic intensity measures (VIII and IX). When comparing the results of Figure 12 with Figure 13, it is clear that the variations are considered smaller for collapse type 2, where different cases are giving 0% variation as shown in street numbers 7, 9, 11, 14, and 15. Although it is considered a critical collapse type, the ESVI values are considered small, since collapse type 2 is reaching high upper limit levels at both seismic intensities. Nevertheless, the results are showing some cases with high variation percentage values that are equal to 80% and 56% as presented in street number 6 at the second zone and 13 at the first zone, respectively. Mainly, the variation in percentages is showing a moderate fluctuation with higher values by changing the seismic intensity scenarios when compared to the assessment approach that is considering the variation of collapse types as shown in Figures 14 and 15.

4.4. Percentage of Variation between Eccentric Seismic Vulnerability Index (ESVI) Values of Seismic Intensity (VIII) for Different Collapse Types. The percentage of variation is calculated by comparing the Eccentric Seismic Vulnerability Index (ESVI) values of a specific seismic intensity (VIII) for the two collapse type scenarios. Figure 14 is showing a small fluctuation of these values when compared to the assessment procedure of the types of collapse at the same seismic intensity. For instance, street numbers 4, 6, and 8 are giving a constant value that is equal to 40% and most of the values are ranging between 23% and 48%. However, the values of variation are considered low when compared to Figures 12 and 13 that focus on assessing the variation percentage for different seismic intensity scenarios. All these described values are reflecting the main results that show a higher effectiveness when changing the seismic intensities in the calculation of the W_{eff} values.

4.5. Percentage of Variation between Eccentric Seismic Vulnerability Index (ESVI) Values of Seismic Intensity (IX) for Different Collapse Types. The percentage of variation values at the specific seismic intensity (IX) based on the difference between collapses type are illustrating the same trend as in Section 4.3, where Figure 15 is illustrating a small fluctuation for these values. For example, street numbers 4, 6, and 8 are giving constant values that are equal to 40% at the three different zones. Moreover, the variation percentages are considered small when compared to the results of Figures 12 and 13, but the values are considered slightly lower than the values that are extracted from Figure 14. This is due to the fact that the variation values at higher seismic intensities are reaching high upper limit levels for both types of collapse.

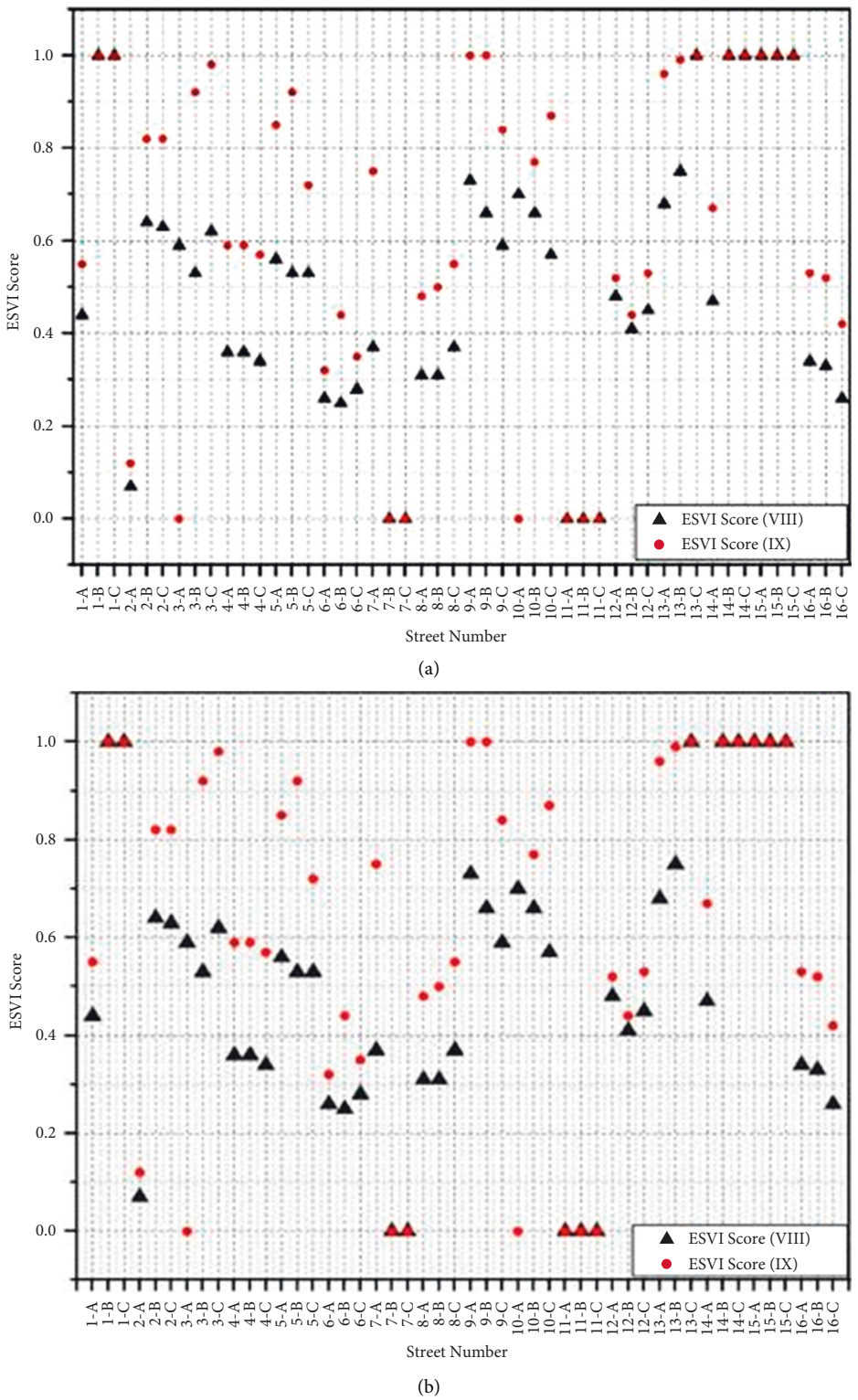

Figure 8: (a) ESVI scores for collapse type 1 at two different seismic intensity scenarios (IX) and (VIII). (b) ESVI scores for collapse type 2 at two different seismic intensity scenarios (IX) and (VIII): A for zone 1, B for zone 2, and C for zone 3.

4.6. Integrated Accessibility Heat Map between Seismic Vulnerability Indices and Resistance Design of the Road. The generated damage maps based on the Intrinsic Seismic Vulnerability Index (ISVI), Eccentric Seismic Vulnerability Index (ESVI), and the integrated seismic vulnerability index maps have shown that it is considered important to reflect the correlation between the intrinsic and eccentric factors, because the generated integrated damage maps are showing less accessibility with high closure probability compared to the singly assessed ESVI and ISVI damage maps. This

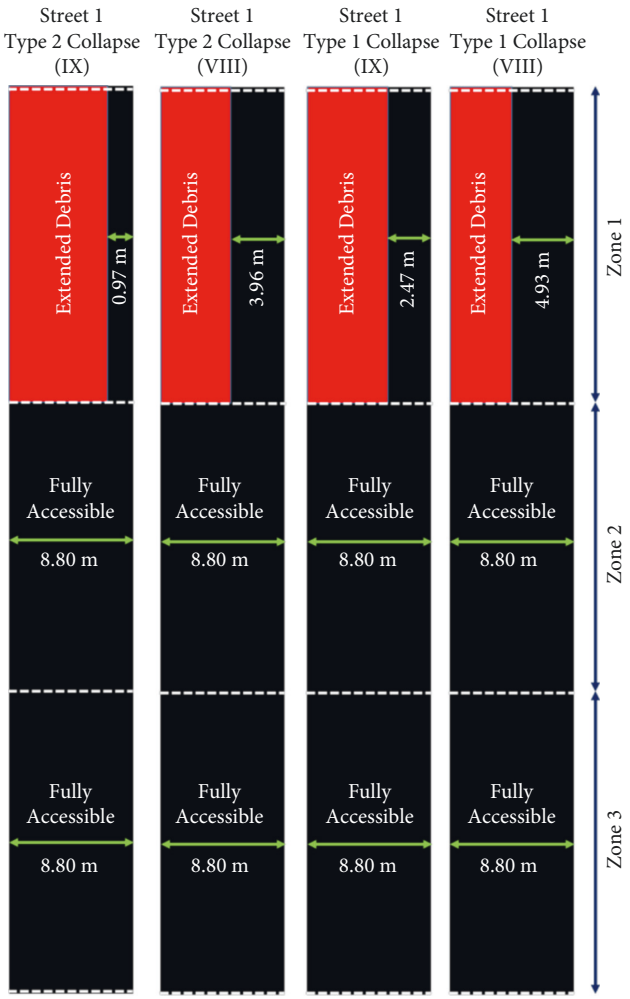

Figure 9: Representative figure for the obstructed zones of street number 1.

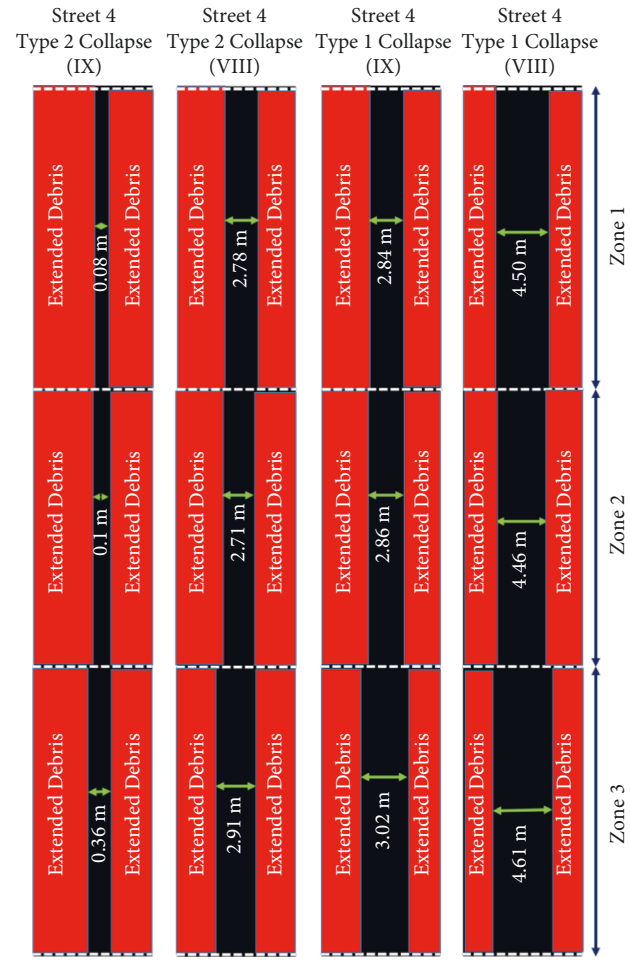

Figure 10: Representative figure for the obstructed zones of street number 4.

correlation can be achieved by developing the integrated accessibility heat maps that are developed in the following sections.

4.6.1. Integrated Accessibility Heat Map Based on the Correlation between Intrinsic Seismic Vulnerability Index (ISVI) and Resistance Design of the Road. The integrated accessibility heat map for Intrinsic Seismic Vulnerability Index (ISVI) is studied based on the correlation with the resistance design of the road, where all the four investigated parameters (embankment heights (P1), pavement strength (P2), the soil type (P3), and number of lanes (P4)) that are studied in Sections 3.1 and 3.2 are taken into consideration, by which the results indicate that the most effective parameter is considered the embankment heights (P1), followed by the number of lanes (P4), while the pavement strength (P2) and soil type (P3) are considered with lower effectiveness rates with a slightly better performance for the soil type.

Figure 16 is illustrating this correlation, by which the results are showing that the Accessibility Index (AI) is gradually decreasing as the ISVI is increasing. However, when analyzing the integrated accessibility heat map, the correlation between both the ISVI and resistance design should be considered. For instance, when investigating the low resistance case, it can be seen that the roads are considered fully accessible when the ISVI is ranging from 0 to 0.1, while when the road system is considered with high resistance design, the road is fully accessible for ISVI ranges between 0 and 0.3. Moreover, the road is considered closed in case of low resistance design when the ISVI is ranging between 0.7 and 1.0. On the other hand, the road is considered closed at higher values of the ISVI for moderate and high resistance design, which are 0.8 and 0.9, respectively. The relation between ISVI and AI is considered inversely proportional, since as the ISVI is increasing, the AI is decreasing. However, this relation is being affected differently based on the situation of the resistance design, where at higher resistance design, the AI is being affected slightly when compared to low and moderate resistance design scenarios.

4.6.2. Integrated Accessibility Heat Map Based on the Correlation between Eccentric Seismic Vulnerability Index (ESVI) and Road Width. Figure 17 illustrates the integrated accessibility heat map through studying the relation between the Eccentric Seismic Vulnerability Index (ESVI) values and

Figure 11: Representative figure for the obstructed zones of street number 10.

number of lanes for the road. This heat map is conducted in case of normal emergency vehicles (NEVs) that are considered with a low manoeuvring limit (2.5 m) than the fast response emergency small vehicles (ESVs) (3.5 m), which is considered in the following section.

The results are showing a high variation between roads with less than two lanes and roads that are with two lanes and above, where the roads with a smaller number of lanes are showing less accessibility. For example, when assessing roads with less than two lanes, the road is considered closed for ESVI values that are ranging between 0.1 and 1.0. However, the roads with two lanes and above are showing higher accessibility, by which the road is considered closed at ESVI values ranging between 0.6 and 1.0 and 0.9 and 1.0 for roads with two lanes and above, respectively. Furthermore, the AI values are considered similar for roads with two lanes and above for ESVI ranges between 0.0 and 0.6, but a slight difference is shown for ESVI values that are ranging between 0.6 and 1.0. It is clear that the wider the road is, the smaller the effect the ESVI is having on the accessibility rates.

On the other hand, when creating the integrated accessibility heat map by studying the relation between ESVI and the number of lanes for ESV, the manoeuvring limit is increased to 3.5 m. Hence, the results and the accessibility rates are varying compared with the heat maps that are created for NEV scenarios as shown in Figure 18. For instance, the roads with less than two lanes are considered closed at the ESVI value equal to 0.3 as shown in ESV heat maps, while for the NEV heat maps, the roads are being closed at a lower ESVI value equal to 0.1. This variation is only represented for road with less than two lanes, but for road with two lanes and above, the AI values are considered the same when comparing the heat maps of NEV and ESV scenarios. Moreover, the same trend is repeated as they created heat maps for NEV, where the results again show that the roads with a smaller number of lanes have lower accessibility rates than those with a higher number of lanes.

4.6.3. Accessibility Heat Maps Based on the Correlation between Integrated Road Characteristics and Integrated SEISMIC Vulnerability Index (SVI). The accessibility heat map is generated by investigating the relation between integrated road characteristics and the integrated seismic vulnerability index that is extracted from the correlation between the ESVI and the ISVI as shown in Figure 19. These are developed for the normal emergency vehicles (NEVs) manoeuvring scenario by studying the integration between the different road characteristics, where the road resistance and the manoeuvring limit is considered during the development of this heat map. The results shown in Figure 19 when compared to Figure 17 are illustrating some variations in the case of a road with two lanes or more, especially when comparing the ESVI and integrated vulnerability index that are ranging between 0.2 and 0.6. This variation is mainly resulting from the followed assessment procedure by which it takes into consideration the integration between the ESVI and ISVI, as well as the integration between different road characteristics.

Figure 20 describes the developed accessibility heat maps by finding the relation between integrated road characteristics and Integrated Seismic Vulnerability Index in the case of the ESV manoeuvring limit scenario. The results are showing a gradual decrease in AI values, where it is giving higher accessibility rates for wider roads with two lanes or more when compared to roads with less than two lanes. However, the results are gradually decreasing and not sharply decreasing as shown in Figure 19. For example, the roadway system with a low resilient design and with less than two lanes is showing a gradual variation for AI with respect to the integrated seismic vulnerability index values, which are ranging between 0.0 and 0.3. Moreover, the roads are closing at higher values when compared to the NEV scenario. Subsequently, the created heat maps that take into consideration the integration between the ESVI and ISVI from one side and the integrated road characteristics from the other side are considered the most efficient maps in the assessment procedure for road networks. This is due to the fact that the integrated maps are focus on all the factors that could affect road network vulnerability and accessibility.

The main findings of this research are achieved by developing an integrated model for road network, by which this research is divided into two parts: the seismic

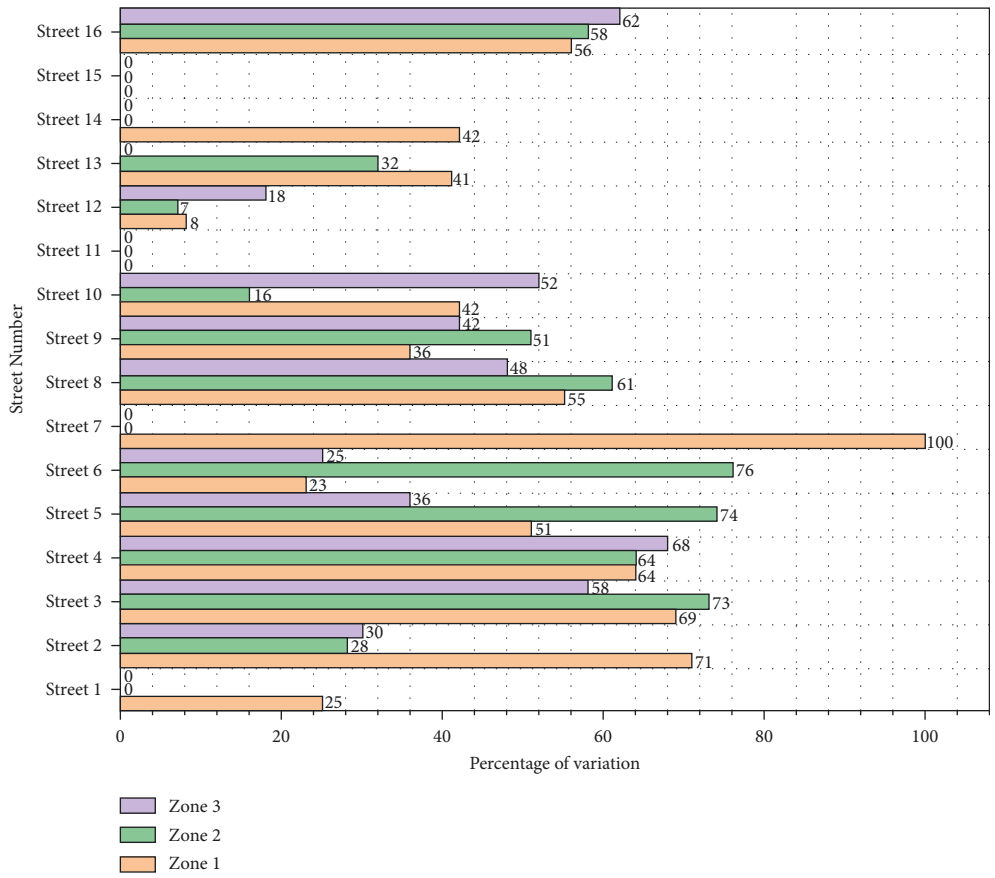

Figure 12: Percentage of variation between ESVI values for collapse type 1 at different seismic intensities.

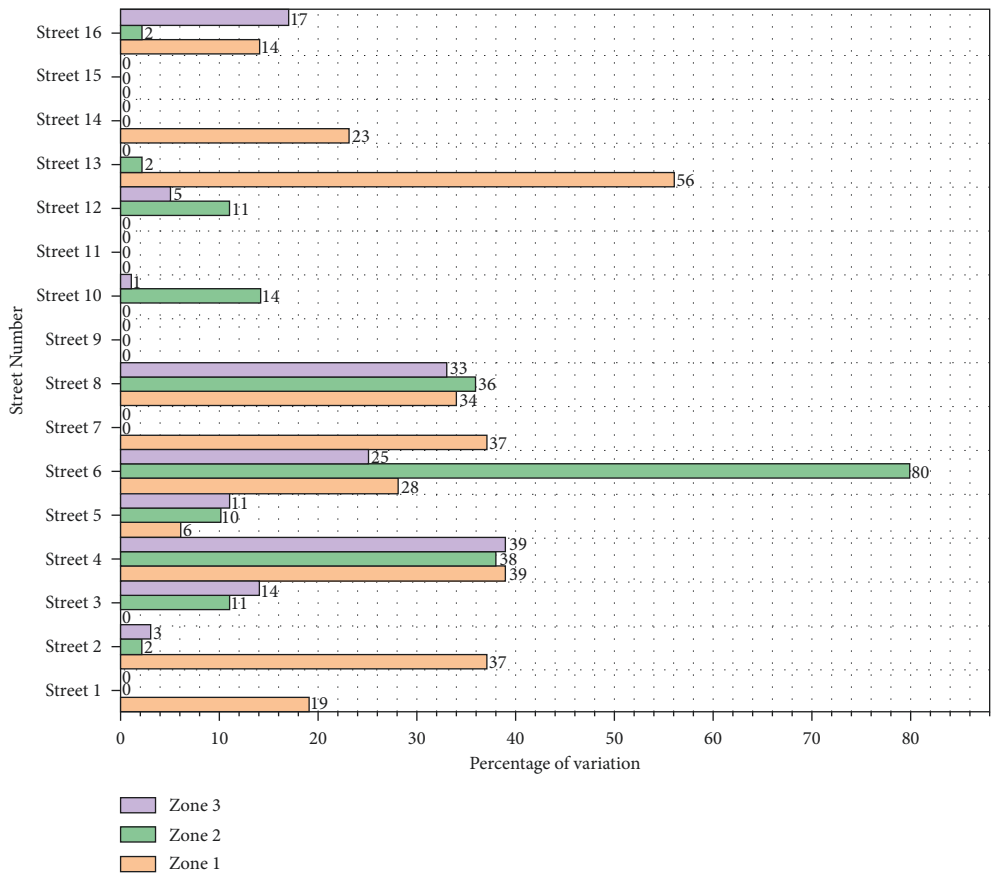

Figure 13: Percentage of variation between effective width ESVI values for collapse type 2 for investigated roads at different seismic intensities.

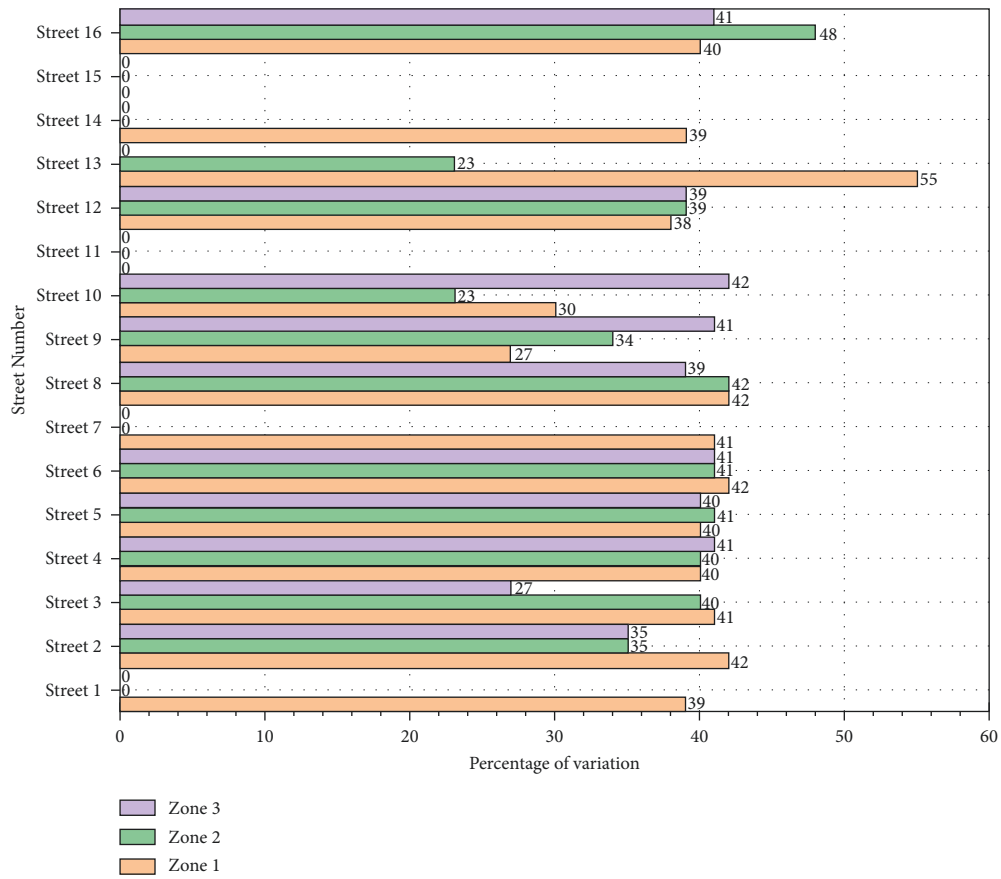

Figure 14: Percentage of variation between effective width ESVI values for collapse type 2 for investigated roads at different seismic intensities.

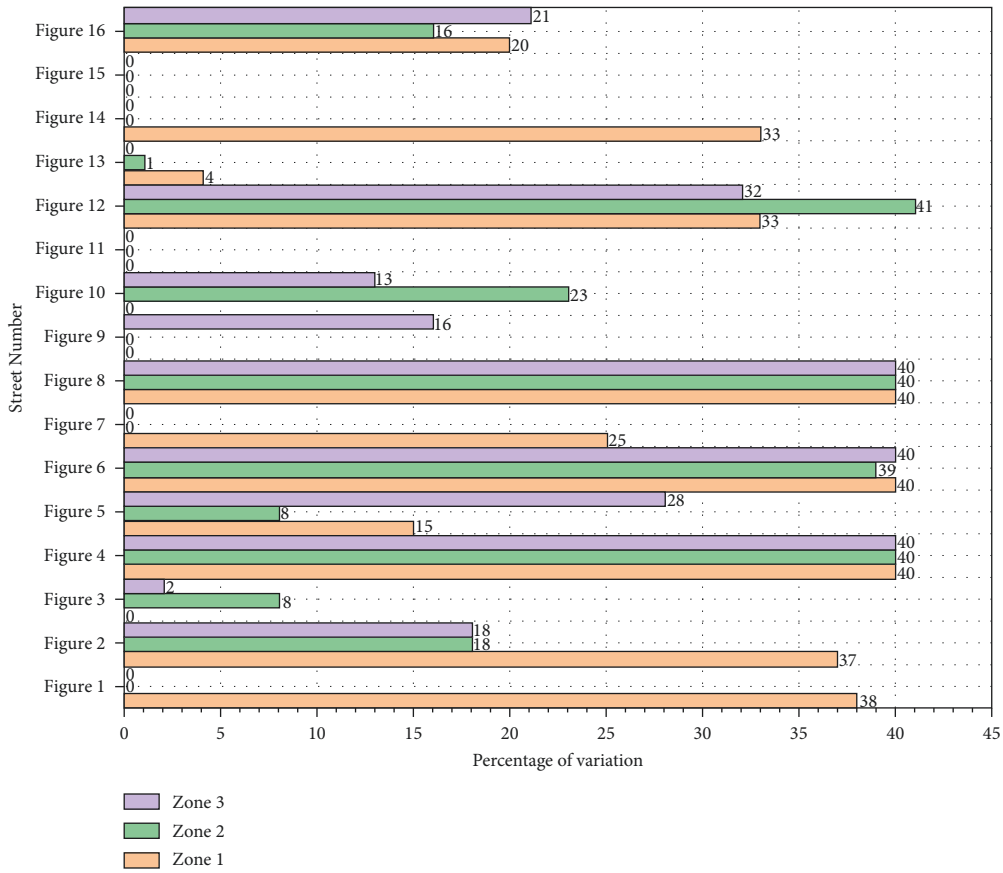

Figure 15: Percentage of variation between ESVI values of seismic intensity IX based on different collapse types.

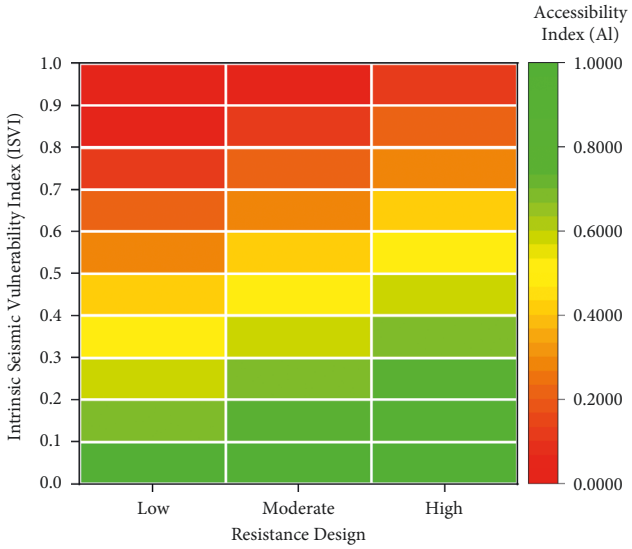

Figure 16: Integrated accessibility heat map between ISVI and resistance design of the road.

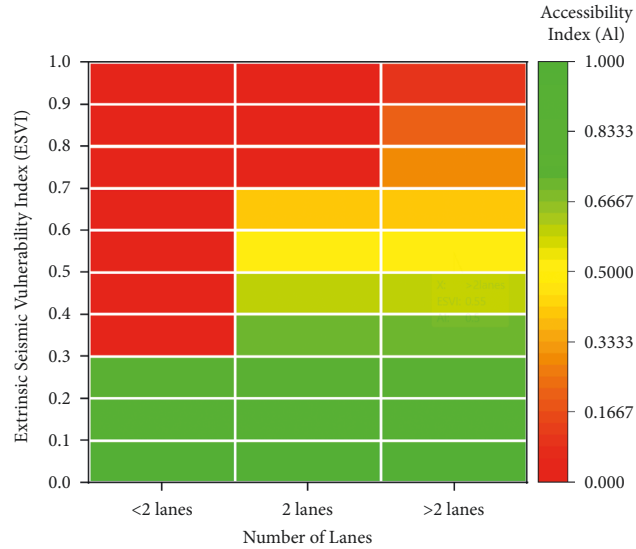

Figure 18: Integrated accessibility heat map between the ESVI and road width of the road for the assessment of ESV.

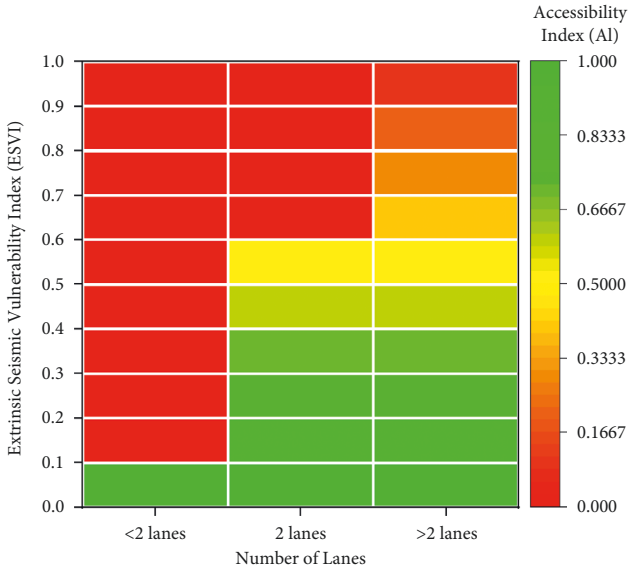

Figure 17: Integrated accessibility heat map between ESVI and road width of the road for the assessment of NEV.

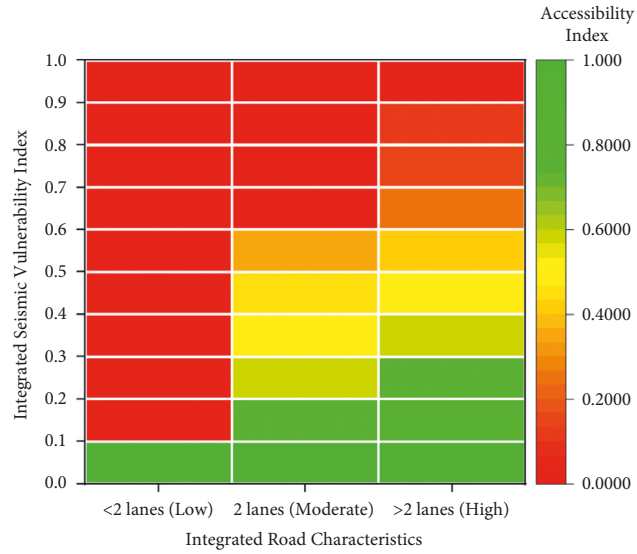

Figure 19: Generated accessibility heat map between integrated road characteristics and integrated seismic vulnerability index for NEVs.

vulnerability indices and the road network accessibility. First of all, this integration model utilized analytical work, which indicated that the number of lanes is considered more efficient when compared to the soil type and height of embankment parameters, but yet deemed more efficient when compared to the pavement strength parameter. This is followed by using the analytical hierarchy process (AHP) method for weighting the values of each parameter that are determined based on the prioritized parameters based on the probability of damage, which in turn develops the Intrinsic Seismic Vulnerability Index (ISVI). However, earthquake debris or road closures can have an impact on roadways as well as the surrounding environment. It is possible to derive a second index, the Eccentric Seismic Vulnerability Index (ESVI), by comparing the width of the debris for two different kinds of collapse. Eventually, an accessibility heat map based on the correlation between integrated road characteristics and the integrated Seismic Vulnerability Index (SVI) is developed.

The aforementioned approach integrates engineering judgment with numerical methods aiming at a comprehensive assessment of the road network accessibility, toward a more efficient emergency planning and improved mitigation strategies for the communities that live in disaster-prone areas.

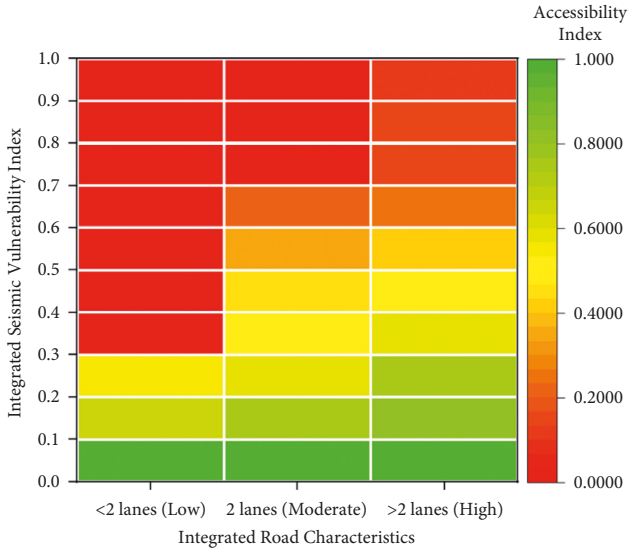

Figure 20: Generated accessibility heat map between integrated road characteristics and integrated seismic vulnerability index for ESV.

5. Conclusion

Through integrating the assessment of intrinsic and eccentric properties, this study assessed the seismic vulnerability of the road network and its interaction with the surrounding buildings. The approach emphasizes the need to combine methodologies to get more exact outcomes, which can help decision-makers lower their exposure to hazardous risk. Furthermore, the significance of this study is in determining the influence of the Intrinsic Seismic Vulnerability Index (ISVI) and Eccentric Seismic Vulnerability Index (ESVI) on road network accessibility when they are investigated separately or as a combined system that is developed in different heat maps. The following are some of the study's findings:

(1) A model that compares the probability of damage (POD) for various collapse states to measure the efficiency of a parameter for assessing the ISVI for road networks and associated assets. The findings demonstrate that the height of the embankment is the most significant parameter, followed by the number of lanes, while the soil type and pavement strength have lower efficiency rates, with soil type having a small superiority.

(2) The effective width (W_{eff}) is retrieved from the data based on the (W_d) assessment, and the W_d values are determined with regard to two different forms of collapse. When compared to standard emergency vehicles, the results show that fast emergency vehicles (ESVs) have higher manoeuvring efficiency and improved functioning levels (NEVs).

(3) Since the resulting integrated damage heat maps reveal less accessibility with a greater closure probability than the singly assessed ESVI and ISVI damage maps, it is crucial to highlight the association between the intrinsic and eccentric properties.

In conclusion, the integrated model can be a powerful tool to increase the disaster preparedness of communities in real-life situations. However, this tool will be more impactful if the multihazard scenarios are considered in the development of this integrated model. Indeed, developing the intrinsic and eccentric vulnerability indices using analytical techniques can reduce or limit the role of the rapid visual screening methods that were used in previous studies based on expert opinion decisions, which depends on observations of damages caused by earthquakes. This can be a useful guide and criterion as an integrated model between traffic accessibility and physical vulnerability to develop a large-scale mapping prior to the earthquake event. Nevertheless, the integrated model is recognized as an innovative tool that can be effective in practical life and in the development of emergency disaster management plans, to avoid fatalities and economic losses following natural hazard occurrences.

Subsequently, future research should focus on the interdependencies of various infrastructures, such as electric power, fuel, transit, airport, or water facilities, as well as the interaction rate between transportation networks and other systems. In this regard, new emerging and digital technologies, as well as resilience analytics, should be enabled in order to develop advanced models.

Data Availability

All the relevant data have been included in the article.

Conflicts of Interest

The authors declare that they have no conflicts of interest.

Acknowledgments

This research was supported by the Ministry of Higher Education Malaysia for Fundamental Research Grant Scheme with project code: FRGS/1/2020/TK02/USM/02/1.

References

[1] A. P. S. Golla, S. P. Bhattacharya, and S. Gupta, "Assessing the discrete and systemic response of the Built Environment to an earthquake," *Sustainable Cities and Society*, vol. 76, Article ID 103406, 2022.

[2] W. R. McClure and T. J. Bartuska, *The Built Environment: A Collaborative Inquiry into Design and Planning*, John Wiley & Sons, Hoboken, NJ, U.S.A, 2011.

[3] W. Miller, "What does built environment research have to do with risk mitigation, resilience and disaster recovery?" *Sustainable Cities and Society*, vol. 19, pp. 91–97, 2015.

[4] G. Andreotti and C. G. Lai, "Use of fragility curves to assess the seismic vulnerability in the risk analysis of mountain tunnels," *Tunnelling and Underground Space Technology*, vol. 91, Article ID 103008, 2019.

[5] S. P. Stefanidou and A. J. Kappos, "Methodology for the development of bridge-specific fragility curves," *Earthquake Engineering & Structural Dynamics*, vol. 46, no. 1, pp. 73–93, 2017.

[6] J. León, C. Mokrani, P. Catalán, R. Cienfuegos, and C. Femenías, "The role of built environment's physical urban form in supporting rapid tsunami evacuations: using computer-based models and real-world data as examination tools," *Frontiers in Built Environment*, vol. 4, p. 89, 2019.

[7] M. H. Rahman, "Earthquakes don't kill, built environment does: e," *Economic Modelling*, vol. 70, pp. 458–468, 2018.

[8] A. P. S. Golla, S. P. Bhattacharya, and S. Gupta, "The accessibility of urban neighborhoods when buildings collapse due to an earthquake," *Transportation Research Part D: Transport and Environment*, vol. 86, Article ID 102439, 2020.

[9] J. M. Andrić, D. G. Lu, "Fuzzy methods for prediction of seismic resilience of bridges," *International Journal of Disaster Risk Reduction*, vol. 22, pp. 458–468, 2017.

[10] C. Huang and S. Huang, "Seismic resilience assessment of aging bridges with different failure modes," *Structures*, vol. 33, pp. 3682–3690, 2021.

[11] L. Sun, D. D'Ayala, R. Fayjaloun, and P. Gehl, "Agent-based model on resilience-oriented rapid responses of road networks under seismic hazard," *Reliability Engineering & System Safety*, vol. 216, Article ID 108030, 2021.

[12] Q. Shang, T. Wang, and J. Li, "A quantitative framework to evaluate the seismic resilience of hospital systems," *Journal of Earthquake Engineering*, vol. 26, no. 7, pp. 3364–3388, 2020.

[13] M. M. Kassem, F. M. Nazri, E. N. Farsangi, and B. Ozturk, "Development of a uniform seismic vulnerability index framework for reinforced concrete building typology," *Journal of Building Engineering*, vol. 47, Article ID 103838, 2022.

[14] M. M. Kassem, F. M. Nazri, E. N. Farsangi, and B. Ozturk, "Improved vulnerability index methodology to quantify seismic risk and loss assessment in reinforced concrete buildings," *Journal of Earthquake Engineering*, pp. 1–36, 2021.

[15] M. M. Kassem, F. M. M. Nazri, and E. N. Farsangi, "The efficiency of an improved seismic vulnerability index under strong ground motions," *Structures*, vol. 23, pp. 366–382, 2020.

[16] S. Adafer and M. Bensaibi, "Seismic vulnerability classification of roads," *Energy Procedia*, vol. 139, pp. 624–630, 2017.

[17] C. Costa, R. Figueiredo, V. Silva, and P. Bazzurro, "Application of open tools and datasets to probabilistic modeling of road traffic disruptions due to earthquake damage," *Earthquake Engineering & Structural Dynamics*, vol. 49, no. 12, pp. 1236–1255, 2020.

[18] K. Ertugay, S. Argyroudis, and H. Ş. Düzgün, "Accessibility modeling in earthquake case considering road closure probabilities: a case study of health and shelter service accessibility in Thessaloniki, Greece," *International Journal of Disaster Risk Reduction*, vol. 17, pp. 49–66, 2016.

[19] S. Argyroudis, J. Selva, P. Gehl, and K. Pitilakis, "Systemic seismic risk assessment of road networks considering interactions with the built environment," *Computer-Aided Civil and Infrastructure Engineering*, vol. 30, no. 7, pp. 524–540, 2015.

[20] Y. Shimura and K. Yamamoto, "Method of searching for earthquake disaster evacuation routes using multi-objective GA and GIS," *Journal of Geographic Information System*, vol. 06, no. 5, pp. 492–525, 2014.

[21] K. Pitilakis, H. Crowley, and A. M. Kaynia, "SYNER-G: Typology Definition and Fragility Functions for Physical Elements at Seismic Risk," *Geological and Earthquake Engineering*, vol. 27, pp. 1–28, 2014.

[22] R. Ferlito and A. Pizza, "A seismic vulnerability model for urban scenarios," *Quick method for the evaluation of roads vulnerability in case of emergency (Modello di vulnerabilità di un centro urbano. Metodologia per la valutazione speditiva della vulnerabilità della viabilità d'em. Ingegneria Sismica*, vol. 4, pp. 31–43, 2011.

[23] B. Shahri, M. Mirzaei, M. Sarrafi, B. Zahabiun, M. Mohaymany, and A. S. Mohaymany, "Transportation network vulnerability analysis for the case of a catastrophic earthquake," *International Journal of Disaster Risk Reduction*, vol. 12, pp. 234–254, 2015.

[24] N. J. Vickers, "Animal communication: when I'm calling you, will you answer too?" *Current Biology*, vol. 27, no. 14, pp. R713–R715, 2017.

[25] P. Luathep, A. Sumalee, H. W. Ho, and F. Kurauchi, "Large-scale road network vulnerability analysis: a sensitivity analysis based approach," *Transportation*, vol. 38, no. 5, pp. 799–817, 2011.

[26] K. A. Hosseini, M. K. Jafari, M. Hosseini, B. Mansouri, and S. Hosseinioon, "Development of urban planning guidelines for improving emergency response capacities in seismic areas of Iran," *Disasters*, vol. 33, no. 4, pp. 645–664, 2009.

[27] G. Caiado, C. Oliveira, M. A. Ferreira, and F. Sá, "Assessing urban road network seismic vulnerability: an integrated approach," in *Proceedings of the 15WCEE*, pp. 24–28, Lisbon, Portugal, September 2012.

[28] A. J. Anastassiadis and S. A. Argyroudis, "Seismic vulnerability analysis in urban systems and road networks. Application to the city of Thessaloniki, Greece," *International Journal of Sustainable Development and Planning*, vol. 2, no. 3, pp. 287–301, 2007.

[29] E. Quagliarini, G. Bernardini, C. Wazinski, L. Spalazzi, and M. D'Orazio, "Urban scenarios modifications due to the earthquake: ruins formation criteria and interactions with pedestrians' evacuation," *Bulletin of Earthquake Engineering*, vol. 14, no. 4, pp. 1071–1101, 2016.

[30] S. Santarelli, G. Bernardini, E. Quagliarini, and M. D'Orazio, "New indices for the existing city-centers streets network reliability and availability assessment in earthquake emergency," *International Journal of Architectural Heritage*, vol. 12, no. 2, pp. 153–168, 2018.

[31] C. Yin, M. M. Kassem, and F. N. Mohamed, "Comprehensive review of community seismic resilience: concept, frameworks, and case studies," *Advances in Civil Engineering*, vol. 2022, Article ID 7668214, pp. 1–19, 2022.

[32] A. M. E. Maissi, S. A. Argyroudis, and F. M. Nazri, "Seismic vulnerability assessment methodologies for roadway assets and networks: a state-of-the-art review," *Sustainability*, vol. 13, no. 1, p. 61, 2020.

[33] S. Argyroudis and A. M. Kaynia, "Analytical seismic fragility functions for highway and railway embankments and cuts," *Earthquake Engineering & Structural Dynamics*, vol. 44, no. 11, pp. 1863–1879, 2015.

[34] T. L. Saaty, "How to make a decision: the analytic hierarchy process," *European Journal of Operational Research*, vol. 48, no. 1, pp. 9–26, 1990.